
Article:
Roberts, D. and Brown, S. (2019) Flow batteries for energy management : novel algebraic modelling approaches to properly assess their value. Journal of Energy Storage, 26. ISSN: 2352-152X

https://doi.org/10.1016/j.est.2019.100977

Flow batteries for energy management: Novel algebraic modelling approaches to properly assess their value

D. Roberts, S. Brown*

Department of Chemical and Biological Engineering, The University of Sheffield, Sheffield S10 2TN

Abstract

Redox Flow Battery (RFB) systems are promising technologies for the multi-hour electrical energy storage that will be necessary for on-demand electricity supply based on wind and solar power. Deriving maximum value from a RFB requires optimisation of both the system design and its operation. In this work three novel algebraic modelling approaches are introduced to represent RFB operation more accurately while maintaining quick optimisation times. First the typical linear programming (LP) optimisation problem is re-posed in terms of current-density rather than power, allowing voltaic losses to be expressed as a quadratic function (QP). Secondly, it is then shown that the current-density framework supports a novel constraint for the avoidance of high cell voltage that may damage the stack. Thirdly, for the first time a binary variable (MIQP) to describe active/idle states is introduced. This allows coulombic leakage and pumping losses to be modelled as fixed terms without constantly draining the RFB, and it allows for the optimisation of pump rating in a VRFB. In a day-ahead energy management case study, it is found that the QP optimisation predicts an additional 19 % annual revenue when compared to the LP optimisation. This capture of the true flexibility of the RFB operation allows its full value to be assessed, and therefore advances the case for their deployment within the energy system. Furthermore, the formulations developed are not only applicable to RFBs but to the scheduling of other battery systems, particularly Li-ion, and balance of plant optimisation, such as the sizing of inverters and climate control systems in the context of parasitic losses.

Keywords: Redox Flow Battery, Optimisation, Mixed Integer Quadratic Programming, Techno-Economic Analysis, Scheduling, VRFB

1. Introduction

Worldwide, the need to reduce CO_2 emissions is stimulating the development of a wide range of renewable energy sources. The growth of renewable energy is forecast to be highest in the electrical power sector, from 24% in 2017

*Corresponding author
Email address: s.f.brown@sheffield.ac.uk (S. Brown)

to 30% in 2023. Although hydro power presently accounts for 50% of renewable power generation, the intermittent power sources wind and solar are forecast to contribute most to this growth (International Energy Agency (IEA), 2018). Indeed, in a number of large European economies, such as Germany, UK, Italy and Spain 23% to 30% of electrical energy was obtained from non-hydro renewable power in 2017 (BP, 2018). In the US, Texas obtained around 17% of electrical energy supply from wind power in 2017, whereas California obtained 9% from wind and 10% from solar (ERCOT, 2017; California Energy Commision, 2018).

To maintain grid stability in these regions, the fluctuating output from wind and solar is supplemented to match demand primarily by varying output from thermal plant. In the UK, this is specifically achieved by closed cycle gas turbines and to a lesser extent coal plant (Drax Group, 2018).

The price of electricity at a given moment is set by the operating costs and finance requirements of the least economic generator that must be called upon to supply it (Staffell and Green, 2016). As wind and solar power have zero marginal cost, or even negative marginal cost where economic incentives are applied, the output of such installations depresses the electricity price intermittently. At the same time, the capacity factors of the dispatchable fossil plant will decrease, and hence a premium is added to their operating cost in order to cover CAPEX and other costs. Across the EU, the operating cost of fossil generation is further increased by the required purchase of credits under the Emissions Trading System (Staffell, 2018). The overall effect of these developments would be an increase in price variability, although this has been mitigated in some markets by capacity payments, made on the basis of power availability rather than energy sold (ENGIE, 2016).

Electricity price variability presents an opportunity for arbitrage by battery energy storage systems (BESS), which may charge and discharge in periods of low and high price respectively. At present however, this revenue alone is not sufficient to justify BESS investment, even under optimistic economic assumptions (Hu et al., 2010). Hence an important aspect of BESS economics is revenue stacking, where multiple revenue streams are captured by the same asset. For example by providing grid reliability services as well as performing market arbitrage. In the UK this is illustrated by the fact that the majority of successful BESS applicants for enhanced frequency response (EFR) contracts also have capacity market contracts (National Grid, 2017).

Sabihuddin et al. (2015) classify the services that BESS may provide by the continuous charge/discharge duration, from power quality and regulation ($< 1\,\mathrm{min}$), through bridging power ($1\,\mathrm{min}$ to $1\,\mathrm{h}$) to energy management ($> 1\,\mathrm{hour}$). In order to satisfy a given duration a BESS must be specified with the corresponding energy to power ratio.

Redox flow battery (RFB) systems are promising candidates for multi-hour applications and revenue stacking, as the incremental cost of energy capacity is low. Systems deployed so far have an average energy to power ratio of 3.5 (Newbery, 2018). In order to quantify the economic merits of RFB systems in comparison to other BESS, or indeed

ESS, it is necessary to perform techno-economic analyses (TEA) for particular applications. TEA should involve optimisation of the operation of a BESS to maximise revenue (or minimise costs). This should be done at various energy and power ratings (as these are decoupled in a non-hybrid RFB) to find the global optimum, as described by Oudalov et al. (2007). The optimisation of operation involves determining the schedule, that is the power input/output of the battery in each sub-period, that maximises benefit without violating energy conservation.

Johnston et al. (2015) used a linear programming (LP) formulation to optimise the scheduling of a vanadium RFB (VRFB) installed at a wind farm. The objective was to maximise revenue on the wholesesale electrical market and the frequency response market, while always maintaining an energy reserve in order to meet mandatory frequency response requirements. By repeating this process at different energy and power ratings, the authors found that increasing the capacity of the VRFB in order to perform additional wholesale market arbitrage is not economical. The authors also suggested that a hybrid system may be suitable, as the economically optimal VRFB operates in a narrow SOC window when providing frequency regulation, with the remaining SOC held in reserve for large frequency deviations that occur infrequently. Vaca et al. (2017) compared a hybrid system consisting of a VRFB and a supercapacitor with the individual systems. They found that the hybrid system was the optimal choice, with the VRFB providing the energy capacity and the supercapacitor the low cost power capacity.

It is worth noting that both Johnston et al. (2015) and Vaca et al. (2017) assume a higher cost of energy capacity than power capacity for the VRFB. This contrasts with earlier modelling of system costs by Viswanathan et al. (2014) and Ha and Gallagher (2015), where the energy cost is markedly lower.

A full system LP schedule optimisation problem was posed by Chen et al. (2012) to assess the benefit of a VRFB in a micro-grid with a load, PV, wind and dispatchable micro-generation. When the micro-grid was isolated, the objective was to minimise the start-up and running costs of micro-generators used to back up the renewable power output. The authors used a mixed-integer LP (MILP) approach, where the integer variables were required to factor start-up costs. Additional global constraints were required to guarantee reliability of the micro-grid.

Gomes et al. (2017) studied the application of a VRFB in order to cope with stochastic deviations from the forecast exports of wind and solar power into a day ahead market. A two stage optimisation was applied, and LP was used to optimise the VRFB schedule based on the forecast in the first stage. Hu et al. (2010) optimised the schedule of a VRFB and a poly-sulphide bromine RFB in order to maximise arbitrage revenue on the Danish day ahead electrical spot market. This approach was not strictly LP, but the problem may be reposed in LP form.

In all of the above studies, the RFB has a fixed state represented by a list of parameters such as round-trip efficiency and maximum charge/discharge power. In reality, these properties are functions of the RFB state at a given moment. For example, the round-trip efficiency parameter is in reality a composite of voltaic and coulombic effi-

ciency, the first of which is dependant on the required current, which in turn depends on the SOC, itself a function of the charge/discharge transactions in all preceding periods. The pursuit of a dynamic model capable of accurately describing the state of an RFB has resulted in a number of approaches, from equivalent circuit models (ECM) using Kalman filters (Mohamed et al., 2013) to a combination of a simplified electrochemical model with an ECM for shunt current losses, and a fluid-dynamics model for pumping losses (Viswanathan et al., 2014) (see Wei et al., 2018, for a summary). However, the complexity of these models restricts their use within a schedule optimisation.

The most detailed representation of an RFB in a schedule optimisation problem is described by Nguyen et al. (2015). The authors apply a previously developed state model (Nguyen et al., 2014) to calculate the state of the RFB at hourly resolution within the optimisation window. The resultant non-convex problem is solved by a search approach with dynamic programming (DP) to break the problem down. This is more computationally intensive than the LP method, but the authors state that an optimum schedule may be found in an acceptable time-scale as the small number of variables and the presence of constraints limit the search space. A DP search approach is also used by Oudalov et al. (2007), where the internal resistance of the BESS is expressed as a function of SOC in a schedule optimisation as part of a TEA of a VRFB and a lead acid battery for industrial peak-shaving.

Sarker et al. (2017) incorporated the dependency of efficiency on power in a MILP scheduling problem (although applied to a Li-ion battery rather than a RFB). To maintain a convex problem, the authors change the boundary definition for the discharge power variable. A piece-wise linear approximation is used to solve the problem. This work is discussed further in section 2.2.

The key innovation of the present work is the introduction of a RFB schedule optimisation framework posed in terms of current-density rather than power. This allows the separation of the voltaic and coulombic components of the power input/output. Using the introduced framework, two dynamic state functions may be posed within the schedule optimisation while maintaining an easily computable convex problem:

- Quadratic expression of ohmic losses (I^2R) in the objective function under linear constraints.
- Maximum cell voltage constraint in terms of OCV and overpotential

In order to further improve the representation of losses we also demonstrate a novel MIQP approach that allows the RFB to be placed in an idle state in order to avoid fixed losses associated with electrolyte pumping and coulombic leakage.

The formulation of each of these elements and the corresponding treatment of the VRFB are described in Section 2. The impact of the improvements to the optimisation formulation are demonstrated in Section 3, using the case study of a $4\,\mathrm{h}$ rated VRFB performing day-ahead energy management on the N2EX electricity market.

2. Model formulation

Pure price arbitrage is chosen as the application for schedule optimisation due to its simplicity, allowing a focus on the treatment of the RFB within the problem. In the following section, an LP formulation for schedule optimisation for maximum arbitrage revenue is first posed in current-density terms to serve as a reference. Then the improvements to the model described in Section 1 are introduced. Finally, the process for specifying the RFB within the problem is defined.

2.1. Reference LP Schedule Optimisation in Current-Density Terms

In the literature on RFB schedule optimisation, scheduling problems are posed using either power (Chen et al. (2012); Hu et al. (2010); Nguyen et al. (2015)) or energy (Johnston et al. (2015); Vaca et al. (2017)) as the time-indexed variables. This is not an important difference, as the former only requires that the timestep τ be included as a coefficient. Here, the power convention is adopted, as it allows the timestep to be varied independently. The objective function for pure arbitrage revenue described by Hu et al. (2010) is adopted here, but adapted so that separate charge and discharge power variables are explicitly defined. Specifying a single power variable with negative values representing charge and positive discharge is not practical for LP optimisation, as the solver will drive the variable to extremes which is likely to be sub-optimal.

In the period Y, made up of sub-periods t, the schedule is optimised by maximising the revenue defined by:

$$R = \frac{\tau}{1 \times 10^6} \sum_{t \in Y} (P_{Dis,t} - P_{Chg,t}) p_t \tag{1}$$

where $P_{Dis,t}$ and $P_{Chg,t}$ represent the bounded variables discharge and charge power (W) between the RFB and the rest of the system in sub-period t. p_t is the price of electrical energy ($£\mathrm{MW}^{-1}\,\mathrm{h}^{-1}$) in sub-period t, and τ the time-step parameter (h).

The SOC of the RFB at time t is defined after Gomes et al. (2017) by:

$$SOC_t = SOC_{t-1} + \frac{\tau P_{Chg,t} \eta_{Chg}}{E_{BESS}} - \frac{\tau P_{Dis,t}}{E_{BESS} \eta_{Dis}} \tag{2}$$

where E_{BESS} is the parameter energy capacity and η_{Chg} and η_{Dis} are the charge and discharge energy efficiency parameters respectively. The SOC must at all times be constrained between a maximum of 1 and a minimum of 0, though a narrower window may be used Vaca et al. (2017).

The above problem was reposed in terms of current-density by replacing the charge/discharge power variables with charge/discharge current-density variables, and multiplying the overall expression by a representative voltage in

order to obtain power input/output by the classical $P = IV$ expression. Current-density was chosen over current as the former is a scale-independent metric commonly used in the RFB literature. The use of current-density makes multiplication by stack area necessary to obtain absolute current. Separate efficiencies representing voltaic and coulombic losses must now be specified, rather than the single energy efficiency term in Equation (2). As current-density is defined based on the current at the RFB terminals, coulombic losses are dealt with upstream in Equation (4). It is however necessary to incorporate voltaic losses in the objective function, as these affect the power input/output. In current-density terms, the LP objective function for arbitrage revenue in period Y to be maximised is defined by:

$$R_{LP} = \frac{A.\tau OCV_{50\%}}{1 \times 10^6} \sum_{t \in Y} p_t (I_{D,t} \sqrt{\bar{\eta}_V}(1 - l_{BOP}) - \frac{I_{C,t}}{\sqrt{\bar{\eta}_V}(1 - l_{BOP})}) \tag{3}$$

where $I_{C,t}$ and $I_{D,t}$ are independent variables representing charge and discharge current density ($\mathrm{A\,m^{-2}}$) respectively. A is the stack area parameter ($\mathrm{m^2}$) and $OCV_{50\%}$ the open cell voltage at 50% SOC. $\bar{\eta}_V$ is the representative round-trip voltaic efficiency. The placement of the additional fractional balance of plant losses parameter l_{BOP} reflects the assumption that balance of plant power consumption is primarily due to electrolyte pumping, and that pumping power is proportional to current. The validity of this assumption is discussed in Section 3.7.

The SOC may now be expressed in purely coulombic terms by replacing the power variables in Equation (2) with current-density variables, the energy efficiency parameters with a coulombic efficiency parameter, and the energy capacity of the RFB with a coulombic capacity. The resultant function for the SOC at the end of sub-period t is defined by:

$$SOC_t = SOC_{t-1} + \frac{A.\tau}{1000C}(I_{C,t}\sqrt{\eta_C} - \frac{I_{D,t}}{\sqrt{\eta_C}}) \; \forall t \in Y \tag{4}$$

where C is the coulombic capacity of the RFB ($\mathrm{A\,h}$). It is assumed that the coulombic efficiency η_C does not vary with SOC or current-density, and that coulombic losses for charge and discharge are symmetrical. This assumption is discussed in Section 3.7.

The following constraints are applied to the list of SOC values generated by the above expression. Firstly the constraint on SOC range is formalised by:

$$SOC_{min} \leq SOC_t \leq SOC_{max} \; \forall t \in Y \tag{5}$$

where SOC_{min} and SOC_{max} are the minimum and maximum permitted SOC parameters.

So that the optimisation may be legitimately performed on consecutive periods of historical data, it is necessary

that the SOC at the end of the period be returned to the starting value. Hu et al. (2010) set this value at 0, but in order to avoid imposing low SOC behaviour, it is here set at 0.5. This constraint is formalised by:

$$SOC_0 = SOC_n = 0.5 \tag{6}$$

where n is the final sub-period in Y.

Finally, the current-density in and out of the RFB is constrained by:

$$0 \leq I_{D,t},\ I_{C,t} \leq I_{max}\ \forall t \in Y \tag{7}$$

where I_{max} is the maximum permitted current-density.

2.2. QP treatment of voltaic losses

A major simplification in the LP problem in terms of power is the assumption of a constant energy efficiency parameter. This assumption also applies to the LP problem in current-density terms introduced in Section 2.1, although separate voltaic and coulombic efficiency parameters are specified. In reality, ohmic (and pseudo-ohmic) over-potential is a linear function of current-density. The faradaic, or activation over-potential, which occurs when the circuit is closed, may be considered constant with respect to current-density Aaron et al. (2011). Equation (3) was adapted to include these losses, by subtracting/adding the faradaic over-potential from/to the OCV during discharge/charge, and including the ohmic losses in the form of the classical $P_{Loss} = I^2R$ equation. This results in a quadratic (QP) objective function for revenue in period Y to be maximised is given by:

$$R_{QP} = \frac{A.\tau}{1 \times 10^6} \sum_{t \in Y} p_t (I_{D,t}(OCV_{50\%} - V_a)(1 - l_{BOP}) - \frac{I_{C,t}(OCV_{50\%} + V_a)}{1 - l_{BOP}} - (I_{D,t}^2 + I_{C,t}^2)ASR) \tag{8}$$

where V_a and ASR are scalar parameters representing faradaic over-potential (V) and area specific resistance ($\Omega\,\mathrm{m}^2$). The simplification of over-potential as a scalar is discussed further in section 3.7. The placement of V_a and ASR reflects an assumption of symmetry in voltaic losses between charge and discharge, which is discussed further in Section 3.7. The objective function is subject to the same constraints as described in Section 2.1.

Although non-linear, the objective function in Equation (8) is convex, as it requires maximising a negative quadratic, hence a gradient based algorithmic solver is guaranteed to find the optimum from any starting point. This is in contrast to the formulation of Nguyen et al. (2015), which is non-convex.

Under the constant coulombic efficiency assumption Equation (4) is linear, and so by extension are the constraints

in Equations (5) and (6). The overall formulation hence comprises a non-linear objective function subject to linear constraints.

This is an improvement over the formulation of losses expressed in power efficiency terms by Sarker et al. (2017), which initially comprises a non-linear objective with a non-linear constraint on SOC. Non-linear constraints are more challenging computationally than non-linear objectives Hart et al. (2017), and the authors apply a piece-wise linear approximation to the efficiency expression. The introduced framework also benefits from a consistent definition of the current-density variables in terms of flow between the terminals and the external system, unlike in Sarker et al. (2017) where, in order to maintain a convex constraint on SOC, the discharge power variable is redefined to be upstream of losses.

2.3. Cell Voltage Constraint

It has so far been assumed that the RFB may accept the maximum charge current-density right up to the maximum permitted SOC. In reality this may result in the cell-voltage being too-high, an issue discussed further in Section 3.4. An alternative charging approach, which is common for Li-ion batteries where high cell voltages pose safety concerns, is to switch to a constant voltage taper charge at high SOC, where the current declines until a cut-off value is reached. In the case of a RFB fixed losses associated with pumping would likely make taper charging uneconomical, as demonstrated by the low efficiency at low current-density reported by Nguyen et al. (2014). Rather than globally adjust the maximum permitted charge current-density or SOC, which may lead to underestimation of revenue, we apply a new linear constraint in terms of cell-voltage, defined by:

$$OCV_t + V_a + I_{C,t} ASR \leq V_{max} \; \forall t \in Y \tag{9}$$

where V_{max} is the maximum permitted cell-voltage and OCV_t is the average open cell voltage in sub-period t, defined by:

$$OCV_t = a\frac{SOC_t + SOC_{t-1}}{2} + b \tag{10}$$

Where a and b are parameters describing the relationship between OCV and SOC in the linear range. This approximation is necessary for tractability; posing eq. (10) via the Nernst equation would result in a non-convex function (as may be observed by inspection). The limitations of this approach are discussed further in section 3.7.

A corresponding constraint for low voltage during discharge could be implemented if required.

2.4. *MIQP model for idling to minimise fixed losses*

The QP model introduced in Section 2.2 makes a simplifying assumption that both the coulombic losses and balance of plant losses are directly proportional to power input/output, via the parameters η_C and l_{BOP}. For this reason the QP optimal schedule in fig. 3a includes periods of low power operation.

In reality neither of these losses behave in this manner. For pumping, the exact behaviour will depend on the system specification: if a constant output pump is employed then the loss will be fixed and hence the efficiency will improve as the power input/output increases. Even if a variable speed pump is employed to avoid unnecessary pump loading there will be a minimum output. For this reason, the pump loss will become relatively large at low power input/output as illustrated by Zeng et al. (2019).

The definition of coulombic losses is more involved, as both shunt currents and active species crossover contribute, and the relative contribution of each will depend on the system. Shunt currents may be modelled using equivalent circuit principles, but even then they will be dependent on cell voltage and electrolyte conductivity, which depends on temperature. Empirically, different VRFB systems display different behaviour. In the experimental work of Lu et al. (2016) and Yuan et al. (2016) the round-trip coulombic efficiency of a VRFB is asymptotic toward 100% as the power input/output increases, implying that the absolute loss is practically constant. However, this trend was only reported for a single cell system, so shunt currents are not included in the analysis. In Reed et al. (2016) the coulombic efficiency of the VRFB stack is practically constant across the studied range of current densities, implying that the absolute coulombic losses increase proportionally to the power input/output. This behaviour may be a consequence of thermal effects, as the system displays an increase in electrolyte temperature with power input/output. This will in principle result in an increased electrolyte conductivity and membrane permeability, both of which may contribute to increased coulombic losses.

In the present work we will model both losses as fixed terms. The potential for developing the model further with more detailed experimental data is discussed in Section section 3.7.

Simply adding a pump power term to eq. (8) and a fixed coulomic loss term to the expression for SOC given in Equation (4) is not a valid solution, as these losses would be present even when the RFB is not performing a service. For this reason it is necessary to add a binary variable to encode idle/active behaviour; we therefore define the objective function by:

$$R_{MIQP} = \frac{\tau}{1 \times 10^6} \sum_{t \in Y} p_t (A(I_{D,t}(OCV_{50\%} - V_a) - I_{C,t}(OCV_{50\%} + V_a) - (I_{D,t}^2 + I_{C,t}^2)ASR) - \delta_t P_{pump}) \quad (11)$$

where δ_t is the Boolean variable indicating idle (0) or active (1) state, and P_{pump} is the fixed pump power (kW),

defined by:

$$P_{pump} = \frac{QdP}{\eta_{pump}} \tag{12}$$

Where Q is the electrolyte flow rate ($\mathrm{l\,s^{-1}}$), dP the pressure drop across the stack (kPa) and η_{pump} the efficiency of the pump. The SOC is then defined by:

$$SOC_t = SOC_{t-1} + \frac{A.\tau}{1000C}(I_{C,t} - I_{D,t} - \delta_t I_{loss})\ \forall t \in Y \tag{13}$$

where I_{loss} is the fixed coulombic loss ($\mathrm{A\,m^{-2}}$).

The charge and discharge current density variables are constrained to be 0 when the system is in the idle state by:

$$\begin{aligned} I_{C,t} - I_{max}\delta_t &<= 0 \\ I_{D,t} - I_{max}\delta_t &<= 0 \end{aligned} \tag{14}$$

a "big M" type constraint, which supercedes the max current constraint posed in eq. (7).

2.5. RFB Specification

The RFB is modelled here as a single cell such that the sizing of the unit may be achieved without the complication of discretisation according to individual electrode area. In our case study stack level phenomena such as shunt currents are captured empirically within the coulombic efficiency data obtained from a stack level experiment. Moving to a different system would require further data, or an offline calculation based on e.g. an equivalent circuit model.

As the power output of any hypothetical RFB may be increased at the cost of efficiency, it is necessary to specify a rated efficiency when determining the stack area required for, say, a $1\,\mathrm{kW}$ system. This is formalised by:

$$\eta_{DC} = \eta_{V,rated}\eta_C(1 - l_{BOP})^2 = \eta_{rated} \tag{15}$$

Where η_V and η_C are the round trip voltaic and coulombic efficiencies respectively. It is assumed that the one-way fractional balance of plant losses (l_{BOP}) are primarily due to electrolyte pumping, and that the pump runs on DC power.

The stack area ($\mathrm{m^2}$) is calculated by:

$$A = \frac{P_{rated}}{I_{rated}OCV_{50\%}\sqrt{\eta_{V,rated}}(1 - l_{BOP})} \tag{16}$$

where P_{rated} is the system power rating (W) and I_{rated} is the current density ($\mathrm{A\,m^{-2}}$) corresponding experimentally to coulombic and voltaic efficiencies that satisfy Equation (15).

The coulombic capacity of the VRFB, required for the tracking of SOC in Equation (4), is calculated by:

$$C = \frac{AI_{rated}r_{e:p}}{\sqrt{\eta_C}(SOC_{max} - SOC_{min})} \tag{17}$$

Where $r_{e:p}$ is the specified energy to power ratio of the system. The presence of η_C ensures there is sufficient chemical energy in the tank to cover coulombic losses upon discharge (square root after Darling et al. (2014)).

3. Case Study

3.1. The Application

Pure price arbitrage on the day ahead N2EX electrical market was chosen as a case study, as the availability of future price information makes deterministic schedule optimisation relevant as described by Hu et al. (2010). Schedule optimisation was performed on 24h periods, with τ of 1h. The indexed price p_t was parametrised using data obtained from the NordPool website Nord Pool (2017).

3.1.1. The RFB

Reed et al. (2016) studied various electrode flow architectures on a $1\,\mathrm{kW}$ VRFB system based on a $50\,\mu\mathrm{m}$ Nafion NR212 membrane. In this case study, performance data were taken from the test of the highest performing stack architecture (IDD2s) at an electrolyte flow rate of 400 $\mathrm{ml\,min^{-1}}$ per cell. This setup was tested at three current-densities: 160, 240 and 320 $\mathrm{mA\,cm^{-2}}$. At each test condition efficiency data were obtained as integrals over a cycle between 15% and 85% SOC.

In the parametrisation of the VRFB for following case studies P_{rated} was set at $1\,\mathrm{kW}$, the energy to power capacity ratio $r_{e:p}$ was set at 4 and η_{rated} was set at 75%. l_{BOP} was set at 0.02, based on a conservative interpretation of the pumping power data reported for a very similar system by Kim et al. (2013). A coulombic efficiency (η_C) of 0.975 was derived as the average of the values reported by Reed et al. (2016) at the three current-densities tested, which only varied between 0.974 and 0.976. For the chosen system the overall energy efficiency requirement in Equation (15) is satisfied when the voltaic efficiency $\eta_{V,rated}$ is 0.801, which corresponds (by linear interpolation) to a current-density (I_{rated}) of $219\,\mathrm{mA\,cm^{-2}}$. $OCV_{50\%}$ was taken from a linear best fit line of data in Kim et al. (2011), where the OCV of a chloride electrolyte was reported at 20%, 50% and 80% SOC. Although a different electrolyte, based on a mixture of sulphuric acid and hydrochloric acid, was used in Reed et al. (2016) the OCV data were not published.

Table 1 summarises the parameter values representing the VRFB in the determination of stack area and coulombic rating.

Table 1: Parameters describing VRFB in sizing process

Param	Value	Units	Source
P_{rated}	1	kW	Arb.
$r_{e:p}$	4	-	Typical
η_{rated}	0.75	-	
$\eta_{V,rated}$	0.801	-	Reed et al. (2016)
η_C	0.975	-	
I_{rated}	219	$\mathrm{mA\,cm^{-2}}$	
A	0.36	$\mathrm{m^2}$	
SOC_{min}	0.15	-	
SOC_{max}	0.85	-	
$OCV_{50\%}$	1.47	V	Kim et al. (2011)
l_{BOP}	0.02	-	Kim et al. (2013)

3.2. Implementation

Each optimisation problem was posed using PYOMO within a Python loop for repeat solutions on 24h sets of data. The gurobi solver (Gurobi Optimization inc., 2018) was called via the SolverFactory module. The script was run on a virtual machine (Oracle, 2018) running Linux Mint, which was allocated 1024 MB RAM.

3.3. QP treatment of Voltaic Losses

In the first case study, the performance of the QP formulation with functionalised voltaic losses (Section 2.2) was assessed by comparison to the LP formulation described in Section 2.1. The LP objective function in Equation (3) requires the assumption of a constant voltaic efficiency term $\bar{\eta}_V$. A value of 0.842 was applied, as this is the voltaic efficiency at the mid-point of the permitted current-density range ($160\,\mathrm{mA\,cm^{-2}}$). Similarly, the QP formulation in Equation (8) requires values for area specific resistance (ASR) and Faradaic potential (V_a) in order to parametrise voltaic losses in the objective function. These were derived by multiplying $OCV_{50\%}$ by $1-\sqrt{\eta_V}$ to obtain an over-potential δ_v at the three current-density points in the experimental data, assuming losses are symmetrical in charge and discharge. ASR was obtained as the gradient of the linear regression on this plot, and V_a as the intercept at zero current-density.

Figure 1 shows the regression of δ_V against current density for the data taken from Reed et al. (2016), from which a value of $0.54\,\Omega\,\mathrm{cm^2}$ was obtained for ASR and a value of $0.03\,\mathrm{V}$ for V_a.

The optimisation of the scheduling was performed for each day in 2017 using both the QP formulation and the LP benchmark. Figure 3a shows the optimal hourly schedule determined by each method for the 14$^{\text{th}}$ of February, and Figure 3b the corresponding SOC profiles. This date is chosen to illustrate the optimisation results because the price profile is typical of a winter day as shown in Section 3.3 and the predicted QP schedule revenue is at the median of the range for the year.

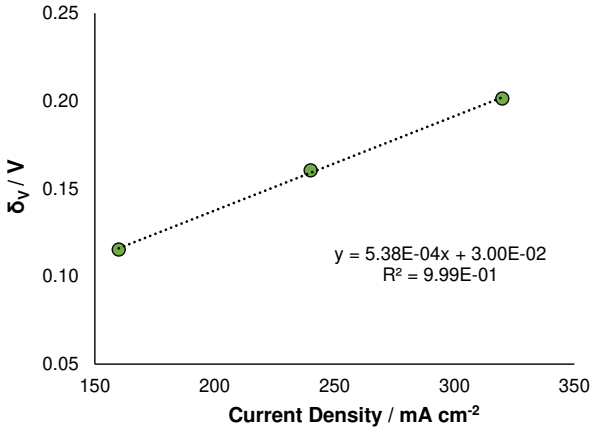

Figure 1: Derivation of ASR (gradient) and V_a (intercept) for IDD2s VRFB embodiment reported by Reed et al. (2016) at 400 $\mathrm{ml\,min^{-1}}$ per cell.

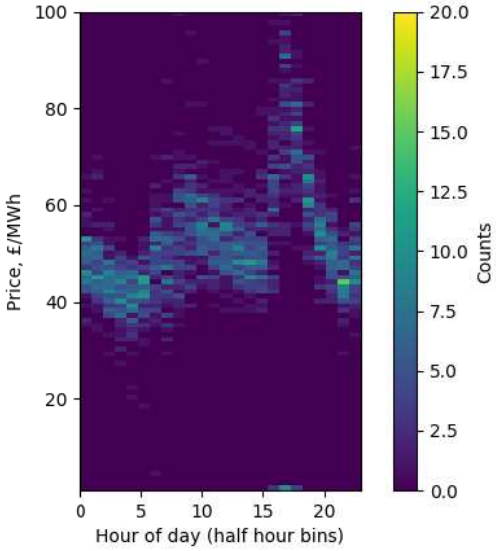

Figure 2: Composite of hourly N2EX day-ahead price data for December, January and February 2017

Both the LP and QP solutions involve charging the VRFB when the electrical price is low (e.g. hours 4 to 6) and discharging it when the price is high (e.g. hours 19 to 21). The LP optimal profile involves discharging or charging the system at high current-density in the four hours with the most extreme prices. The QP optimal schedule also targets the most extreme periods, but spreads the charging/discharging out. This is the consequence of factoring variable ohmic losses in the objective function, where high current-density is penalised by higher losses.

The practical economic implications of applying the QP approach in this case study are discussed in section 3.6.

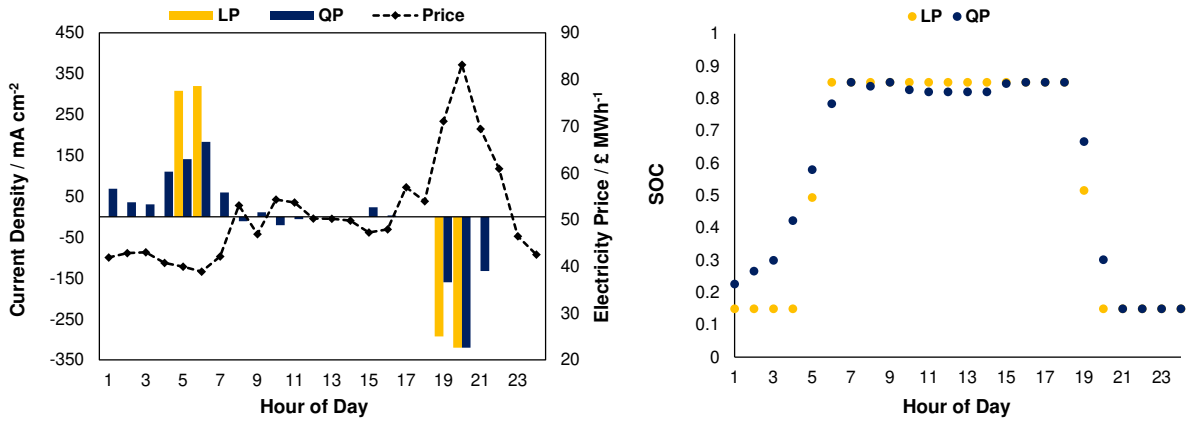

(a) (b)

Figure 3: (a) Optimal VRFB schedules derived for the 14th February 2017 using LP and QP optimisation formulations (discharge plotted as negative). (b) corresponding SOC values. Note that the N2EX day-ahead window runs from 23:00 to 23:00.

3.4. QP with Cell-Voltage constraint

In the LP and QP formulations given in Sections 2.1 and 2.2 it is assumed that the RFB may be charged at maximum current-density at the maximum SOC. This was the charging strategy applied by Reed et al. (2016), where the cell-voltage was allowed to reach $1.85\,\mathrm{V}$ at the highest current-density, corresponding to an approximate SOC of 0.85. Overcharging may lead to oxygen evolution at the cathode and hydrogen evolution at the anode. This results in reduced coulombic efficiency and, more importantly, the evolved gases can cause a range of problems as described by Kear et al. (2012) and Wei et al. (2018). The particular cell-voltage at which gas evolution becomes problematic will depend on the particular electrode and electrolyte chemistry of the system.

In this case study V_{max} in Equation (9) was set at 1.65, just below the voltage at which Wei et al. (2017) reported evolution of macroscopic bubbles of hydrogen and oxygen ($1.70\,\mathrm{V}$). The parameters a and b representing the linear relationship between OCV and SOC described in eq. (10) were set at 0.267 and 1.33 respectively Kim et al. (2011).

Figure 4a shows the optimal schedules with and without constraint for 5th February 2017, where the difference in revenue was greatest (£$0.18\,\mathrm{kW}^{-1}$ vs. £$0.20\,\mathrm{kW}^{-1}$). Figure 4b shows the corresponding cell-voltage profiles.

In the unconstrained case the RFB charges at the maximum current-density of $320\,\mathrm{mA\,cm}^{-2}$ in hour 20 in order to capitalise on the unusually low electrical price, resulting in a cell-voltage of $1.71\,\mathrm{V}$. In the constrained case, the current-density is restricted to $221\,\mathrm{mA\,cm}^{-2}$ in the same period, and the RFB must charge more (and discharge less) in other periods to satisfy Equation (6).

Maximising Equation (8) subject to Equation (9) for the 2017 data resulted in £$30.11\,\mathrm{kW}^{-1}$ compared to £$30.22\,\mathrm{kW}^{-1}$

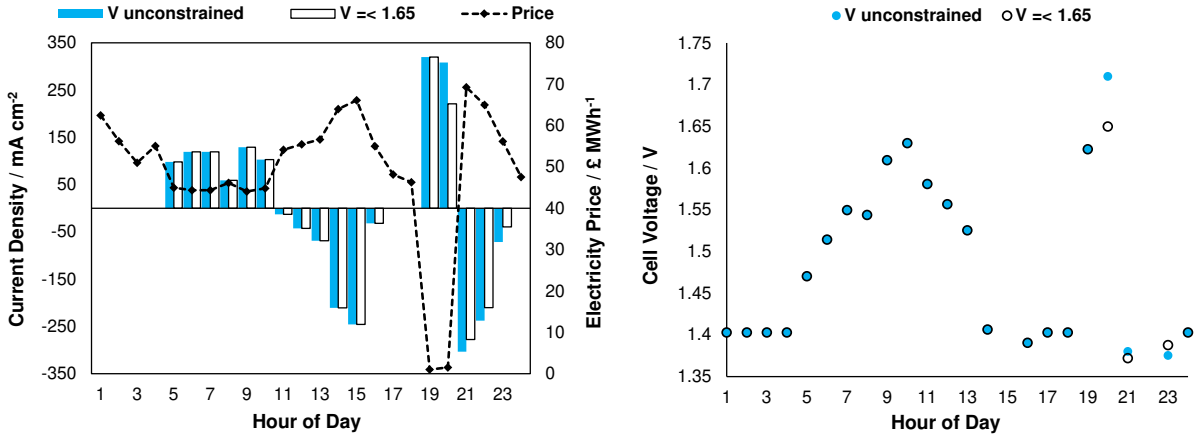

Figure 4: (a) Optimal VRFB schedules derived for the 5th February 2017 by maximising Equation (8) with no cell-voltage constraint, and subject to the cell voltage constraint given in Equation (9). (b) Corresponding cell-voltage profiles.

when the cell voltage was not constrained. The difference is small because high current-density is already discouraged by the factoring of voltaic losses in the objective function.

The impact of the constraint would be more severe if the variations in price data were greater, or the maximum voltage set at a lower value. The constraint would also become more relevant if the timestep τ were decreased, as higher average intra-period SOC values would be returned in eq. (10).

The application of the linear constraint on cell-voltage increases the time to process the 2017 data as shown in Table 3.

3.5. MIQP treatment of fixed losses and idling

Table 2 shows the parameters used to represent the fixed losses in the MIQP formulation. In the Reed et al. (2016) study, for a given electrolyte flow rate the pressure drop decreases as the current density increases, due to the reduction in electrolyte viscosity with increasing temperature. However, for the IDD2s flow design, the pressure drop is only reported for the lowest current density set point, so the estimate is conservative. The flow rate is arrived at by multiplying the 400 $\mathrm{ml\,min^{-1}}$ per cell set point in Reed et al. (2016) by the 5 cells that would be required to arrive at the specified stack area in Table 1, given the 0.078 $\mathrm{m^2}$ cell area. The fixed coulombic loss was estimated from the round trip coulombic efficiency at 240 $\mathrm{mA\,cm^{-2}}$, assuming symmetrical losses.

The MIQP optimisation was performed over the 2017 day-ahead dataset. The optimal schedule for the representative winter day is compared to the QP and LP solutions in fig. 5a.

These results show that the introduced MIQP formulation allows fixed losses to be posed so that unrealistic low

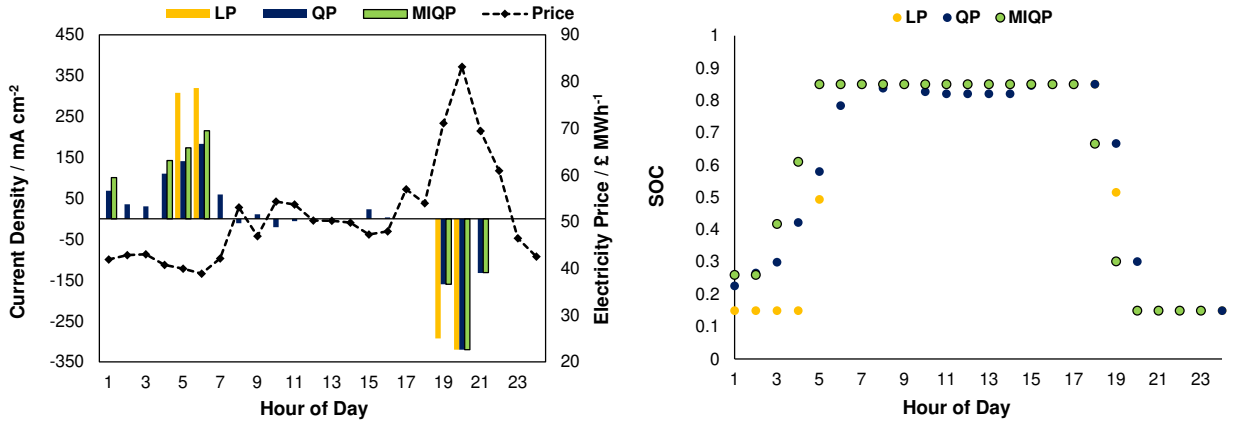

(a) (b)

Figure 5: (a) Optimal VRFB schedules derived for the 14th February 2017 using the LP, QP and MIQP formulations (all at the 0.33 $\mathrm{l\,s^{-1}}$ electrolyte flow rate in (Reed et al., 2016)). (b) Corresponding SOC profiles.

power behaviour is avoided. The economic implications of this development are discussed in section 3.6.

3.6. Practical benefits of the introduced formulations.

As mentioned in section 3.3, a major limitation of LP schedule optimisation formulation is the failure to account for the dependence of voltaic efficiency on current-density. In the above case study, we used the voltaic efficiency at the middle of the permitted current-density range as a representative value. It is of course possible to set different values for the efficiency, for example using the efficiency at maximum current density as a worst case scenario. However, the optimal schedule obtained for a given day is the same whatever value is set. By inputting the LP optimal schedules into the QP objective function it is therefore possible to estimate the revenue not accounted for using the latter approach. We calculate this to be 19%, going from £25.58 $\mathrm{kW^{-1}}$ to £30.32 $\mathrm{kW^{-1}}$ across the 2017 data.

Unfortunately it is not possible to run the LP or QP solutions through the MIQP objective function, because the change to the coulombic treatment from eq. (4) to eq. (13) means that the assumptions regarding the SOC would be false. In any case, further experimental data is required to determine more rigorously the relationship between coulombic leakage and current-density.

The MIQP formulation opens up the possibility of more detailed optimisation regarding balance of plant. Reed et al. (2016) reported efficiency data for three different flow rates, alongside the stack pressure drop. The voltaic losses decreased as flow rate increased. The MIQP formulation can be used to determine which flow rate is most appropriate for our case chosen case study. The parameters associated with each set point are shown in table 2. A pump efficiency of 0.6 was assumed in all cases.

Q ($\mathrm{l\,s^{-1}}$)	dP (kPa)	ASR $\mathrm{m\Omega\,cm^{-2}}$	V_a (V)	I_{loss} ($\mathrm{mA\,cm^{-2}}$)	P_{pump} (W)
0.033	34	5.4	0.03	2.9	1.9
0.067	55	5.2	0.02	3.0	6.1
0.100	90	5.0	0.02	3.6	15

Table 2: Efficiency parameters for MIQP representation of Reed et al. (2016) VRFB at different flow rates.

The optimal schedules for each flow rate on 14th February 2017 are shown in fig. 6a. There is little change to the schedule on going from 0.33 $\mathrm{l\,s^{-1}}$ to 0.67 $\mathrm{l\,s^{-1}}$ but the sharp increase in pressure drop to the 1.00 $\mathrm{l\,s^{-1}}$ set-point makes the low power charging seen at lower flow rates in hour 1 sub-optimal.

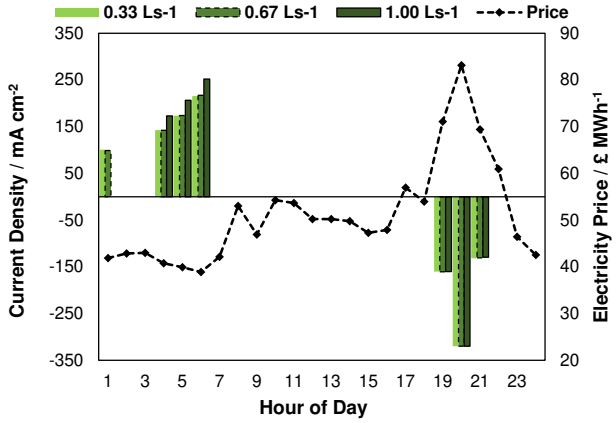

(a)

Figure 6: MIQP optimal VRFB schedules derived for the 14th February 2017 under the different electrolyte flowrates reported by Reed et al. (2016).

The schedule optimisation was repeated for each day in 2017 for the increased flow rate cases. Increasing the flow rate from 0.33 to $\mathrm{l\,s^{-1}}$ to 0.67 $\mathrm{l\,s^{-1}}$ increased the predicted revenue slightly from £32.57 $\mathrm{kW^{-1}}$ to £33.56 $\mathrm{kW^{-1}}$ but going to 1.00 $\mathrm{l\,s^{-1}}$ reduced it to £32.17 $\mathrm{kW^{-1}}$. In reality, the small benefit of the increased flow rate may be outweighed by the cost of the additional pump capacity.

The solution time for each of the formulations that have been introduced in this article are shown in Table 3 alongside the LP benchmark. While the treatment of variable voltaic losses using the QP formulation results in a minimal increase to the solve time, the addition of a cell voltage constraint does slow the process. The MIQP functionality for active/idle behaviour further slows the optimisation, but solving for each 24h scenario still takes less than 1 s.

3.7. Analysis of Assumptions

There are a number of assumptions remaining in our treatment of the RFB in schedule optimisation:

1. In eq. (8) the faradaic over-potential is modelled as a scalar, which is obtained by extrapolating the linear section

Formulation	Unconstrained Voltage	Dynamic Upper Voltage Constraint
LP	129	n/a
QP	132	176
MIQP	170	239

Table 3: Solution times (s) to optimise RFB schedule against 2017 day-ahead price data 24h hour at a time. Average of two runs including Python script time.

of the polarisation curve to zero current density (as shown in fig. 1). This ignores the logarithmic relationship between over-potential and current, defined by the Butler-Volmer equation. It would be possible to provide a better approximation of the over-potential via a piecewise linearisation of the logarithmic function, but this would slow the computation time. As low current operation (where the approximation is poorest) is already discouraged by parasitic losses, it is not expected that improving the kinetic model would have a meaningful impact on either the optimum schedule or the revenue.

2. It is assumed that both coulombic efficiency and the voltaic loss parameters are invariant with SOC and symmetrical, i.e. the same for charge and discharge. Regarding the first assumption, experimental work by Nguyen et al. (2014) showed that the voltaic discharge efficiency is lower at 70% SOC than at 35% SOC, but that the difference decreases as power increases, although data are only reported up to $1.8\,\mathrm{kW}$ for a $5\,\mathrm{kW}$ system. Regarding the latter, the same authors provide experimental evidence that the voltaic efficiency of the particular VRFB is higher for charge than discharge. The latter issue could be dealt with easily in the present formulation, if experimental data were made available, by applying separate ASR, V_a and η_C terms for charge and discharge. The former issue would be more difficult to deal with, as making ASR of V_a a function of SOC would result in a non-convex objective function and doing so for η_C would yield a non-convex constraint. A first step would be to perform a sensitivity study based on relevant system data.
3. In the introduced formulation a fixed OCV is assumed in the objective function, based on the value at 50% SOC. Although in reality OCV is a function of SOC, defining it as such would result in a non-convex objective function, which may require a search approach as in Nguyen et al. (2015). It is assumed that operation at low SOC and high SOC will balance out, as the system must return to the same SOC at the end of each day. For the case study in Section 3.3, adjusting the revenue calculation to account for the actual OCV that would occur in each sub-period results in a very small increase to 2017 revenue, from $£28.07\,\mathrm{kW}^{-1}$ to $£28.28\,\mathrm{kW}^{-1}$.
4. It is assumed for the purposes of this demonstration that pumping and coulombic losses are fixed terms. In reality this is not the case, and the degree with which our simplified formulation fits the reality will depend on the specifics of the system. In the case of the Reed et al. (2016) system, the absolute coulombic loss increases with current density, but it would be necessary to test the system at lower current densities to better understand

the empirical behaviour, and whether a linear or quadratic function should be added to eq. (13).

5. The RFB is not thermally constrained. The VRFB based on a sulphate electrolyte is liable to precipitation of V_2O_5 from the catholyte as temperature increases (Rahman and Skyllas-Kazacos, 2009; Vijayakumar et al., 2011). Although the chloride and mixed acid electrolytes developed at PNNL are more stable (Li et al., 2011; Kim et al., 2011), temperature remains an important consideration. The framework introduced here could be expanded to capture the thermal performance of the system. A thermal constraint could be put in place using a similar construct to the one describing SOC, where voltaic losses add heat to the electrolyte and active or passive cooling removes it. This would allow cost benefit analyses of active cooling versus restrictions on operation in different environmental conditions.
6. In the case study the RFB is overly constrained in terms of SOC, being limited to the range in which the OCV depends linearly upon it (0.15 to 0.85 based on the Reed et al. (2016) system). Frequent access to full depth of discharge with no performance degradation is an often highlighted benefit of VRFB systems. However, it is more difficult to avoid mass transfer limitations at extreme SOC, as the unreacted species become diluted. Hence either higher pumping power must be supplied, power input/output restricted or voltaic efficiency compromised. A fuller study of this issue could be carried out by applying piece-wise treatment of voltaic efficiency and the cell voltage constraint.

4. Conclusion

A novel framework for RFB schedule optimisation has been introduced in which the voltaic and coulombic components of the power output/input are separated, with the problem variablised in terms of current-density. A day ahead energy management case study is used to demonstrate the increased fidelity that is achievable using the framework.

The framework is first used to describe ohmic losses as a quadratic function of current-density in the objective function, while maintaining a convex solution space and all linear constraints. The importance of inclusion of variable ohmic losses in the arbitrage case study is demonstrated. The optimal deterministic schedule computed using the introduced formulation (QP) would result in a 19% greater revenue across 2017 when compared to a basic LP approach that assumes a constant representative voltaic efficiency. This represents considerable value that the LP approach fails to recognise because of the constant efficiency assumption.

The fidelity of the RFB representation is further increased by placing a novel linear constraint on cell-voltage as a function of SOC and over-potential. This constraint restricts the current-density at which the battery may be charged when the SOC is high, which is an important consideration for safety and battery lifetime. In the present case study, the impact of the chosen maximum voltage is low, as the previous factoring of voltaic losses already discourages high power input. However, in other applications this constraint will become more important. Although the present work

has focused on RFB systems, the easy application of cell-voltage constraint would be useful for Li-ion scheduling, where low and high cell-voltages increase cell degradation, and the latter also poses a safety concern.

Finally, a MIQP model that captures active/idle behaviour has been introduced for the first time, allowing a more realistic representation of losses that do not scale proportionally with current-density. The usefulness of this approach in electrolyte flow rate optimisation has been demonstrated here, but there are other interesting applications. Inverter sizing is one of these: installing a larger inverter allows a greater maximum power output, but will incur a greater fixed loss. Similarly, installing climate control for more extreme locations will allow more intensive operation without breaching thermal constraints, but again there will be a parasitic loss. These problems are applicable to both VRFB and Li-ion systems.

It is intended that the novel framework be used for TEA and optimisation of various RFB chemistries at a system level (i.e. up to the AC-DC boundary), for example in the optimal specification of pump rating, or climate control system for a particular application. RFB systems have previously been the subject of technical optimisation, for example the study of the trade-offs between electrolyte concentration and ASR (Cho et al., 2013), or shunt currents and pumping losses (Viswanathan et al., 2014). In these works, a simple metric such as levelised cost of electrical energy under a simple duty cycle is used as the objective to minimise. The framework introduced here allows optimisation in terms of revenue under optimal scheduling for any application where a price signal exists.

5. Acknowledgements

This work was supported by the UK Engineering and Physical Science Research Council via grant EP/L016818/1 which funds the Centre for Doctoral Training in Energy Storage and its Applications. The authors are also grateful to Drax Power Ltd. for their financial support.

References

Aaron, D., Tang, Z., Papandrew, A. B., Zawodzinski, T. A., oct 2011. Polarization curve analysis of all-vanadium redox flow batteries. Journal of Applied Electrochemistry 41 (10), 1175–1182.

BP, 2018. BP Statistical Review of World Energy. Tech. rep.

California Energy Commision, 2018. Total system electric generation.
URL https://www.energy.ca.gov/almanac/electricity_data/total_system_power.html

Chen, S. X., Gooi, H. B., Wang, M. Q., mar 2012. Sizing of energy storage for microgrids. IEEE Transactions on Smart Grid 3 (1), 142–151.

Cho, K. T., Albertus, P., Battaglia, V., Kojic, A., Srinivasan, V., Weber, A. Z., 2013. Optimization and Analysis of High-Power Hydrogen/Bromine-Flow Batteries for Grid-Scale Energy Storage. Energy Technology 1 (10), 596–608.

Darling, R. M., Gallagher, K. G., Kowalski, J. A., Ha, S., Brushett, F. R., sep 2014. Pathways to low-cost electrochemical energy storage: a comparison of aqueous and nonaqueous flow batteries. Energy Environ. Sci. 7 (11), 3459–3477.

Drax Group, 2018. Drax Electric Insights.
URL www.electricinsights.co.uk

ENGIE, 2016. Understanding the (UK) Capacity Market. Tech. rep.
URL http://business.engie.co.uk/wp-content/uploads/2016/07/capacitymarketguide.pdf

ERCOT, 2017. ERCOT Quick Facts for 2017. Tech. rep.
URL https://www.dropbox.com/s/vcrbv143x9u8y6c/ERCOT_Quick_Facts_for_2017_2518.pdf?dl=0

Gomes, I. L., Pousinho, H. M., Melício, R., Mendes, V. M., apr 2017. Stochastic coordination of joint wind and photovoltaic systems with energy storage in day-ahead market. Energy 124, 310–320.

Gurobi Optimization inc., 2018. Mathematical Programming Solver | Gurobi.
URL http://www.gurobi.com/products/gurobi-optimizer

Ha, S., Gallagher, K. G., 2015. Estimating the system price of redox flow batteries for grid storage. Journal of Power Sources 296, 122–132.

Hart, W. E., Laird, C. D., Watson, J.-P., Woodruff, D. L., Hackebeil, G. A., Nicholson, B. L., Siirola, J. D., 2017. Pyomo - Optimization Modeling in Python, 2nd Edition. Vol. 67 of Springer Optimization and Its Applications. Springer.

Hu, W., Chen, Z., Bak-Jensen, B., jul 2010. Optimal operation strategy of battery energy storage system to real-time electricity price in Denmark. In: IEEE PES General Meeting, PES 2010. IEEE, pp. 1–7.

International Energy Agency (IEA), 2018. Renewables 2018.
URL https://www.iea.org/renewables2018/

Johnston, L., Díaz-González, F., Gomis-Bellmunt, O., Corchero-García, C., Cruz-Zambrano, M., jan 2015. Methodology for the economic optimisation of energy storage systems for frequency support in wind power plants. Applied Energy 137, 660–669.

Kear, G., Shah, A. A., Walsh, F. C., sep 2012. Development of the all-vanadium redox flow battery for energy storage: A review of technological, Financial and policy aspects. International Journal of Energy Research 36 (11), 1105–1120.

Kim, S., Thomsen, E., Xia, G., Nie, Z., Bao, J., Recknagle, K., Wang, W., Viswanathan, V., Luo, Q., Wei, X., Crawford, A., Coffey, G., Maupin, G., Sprenkle, V., sep 2013. 1 kW/1 kWh advanced vanadium redox flow battery utilizing mixed acid electrolytes. Journal of Power Sources 237, 300–309.

Kim, S., Vijayakumar, M., Wang, W., Zhang, J., Chen, B., Nie, Z., Chen, F., Hu, J., Li, L., Yang, Z., 2011. Chloride supporting electrolytes for all-vanadium redox flow batteries. Physical Chemistry Chemical Physics 13 (40), 18186.

Li, L., Kim, S., Wang, W., Vijayakumar, M., Nie, Z., Chen, B., Zhang, J., Xia, G., Hu, J., Graff, G., Liu, J., Yang, Z., may 2011. A stable vanadium redox-flow battery with high energy density for large-scale energy storage. Advanced Energy Materials 1 (3), 394–400.

Lu, W., Yuan, Z., Zhao, Y., Li, X., Zhang, H., Vankelecom, I. F., jul 2016. High-performance porous uncharged membranes for vanadium flow battery applications created by tuning cohesive and swelling forces. Energy and Environmental Science 9 (7), 2319–2325.

Mohamed, M. R., Ahmad, H., Seman, M. N., Razali, S., Najib, M. S., 2013. Electrical circuit model of a vanadium redox flow battery using extended Kalman filter. Journal of Power Sources 239, 284–293.

National Grid, 2017. Duration-Limited Storage De-Rating Factor Assessment âĂŞ Final Report. Tech. Rep. November.

Newbery, D., feb 2018. Shifting demand and supply over time and space to manage intermittent generation: The economics of electrical storage. Energy Policy 113, 711–720.

Nguyen, T. A., Crow, M. L., Elmore, A. C., jul 2015. Optimal sizing of a vanadium redox battery system for microgrid systems. IEEE Transactions on Sustainable Energy 6 (3), 729–737.

Nguyen, T. A., Qiu, X., Guggenberger, J. D., Crow, M. L., Elmore, A. C., oct 2014. Performance characterization for photovoltaic-vanadium redox battery microgrid systems. IEEE Transactions on Sustainable Energy 5 (4), 1379–1388.

Nord Pool, 2017. Historical Market Data.
URL https://www.nordpoolgroup.com/historical-market-data/

Oracle, 2018. Downloads - Oracle VM VirtualBox.
URL https://www.virtualbox.org/wiki/Downloads

Oudalov, A., Cherkaoui, R., Beguin, A., jul 2007. Sizing and optimal operation of battery energy storage system for peak shaving application. In: 2007 IEEE Lausanne POWERTECH, Proceedings. IEEE, pp. 621–625.

Rahman, F., Skyllas-Kazacos, M., apr 2009. Vanadium redox battery: Positive half-cell electrolyte studies. Journal of Power Sources 189 (2), 1212–1219.

Reed, D., Thomsen, E., Li, B., Wang, W., Nie, Z., Koeppel, B., Kizewski, J., Sprenkle, V., 2016. Stack Developments in a kW Class All Vanadium Mixed Acid Redox Flow Battery at the Pacific Northwest National Laboratory. Journal of The Electrochemical Society 163 (1), A5211–A5219.

Sabihuddin, S., Kiprakis, A. E., Mueller, M., dec 2015. A numerical and graphical review of energy storage technologies. Energies 8 (1), 172–216.

Sarker, M. R., Murbach, M. D., Schwartz, D. T., Ortega-Vazquez, M. A., nov 2017. Optimal operation of a battery energy storage system: Trade-off between grid economics and storage health. Electric Power Systems Research 152, 342–349.

Staffell, I., 2018. Coal comeback pushes up UK's carbon emissions - Drax.
URL https://www.drax.com/energy-policy/electric-insights-coal-comeback-pushes-up-uk-carbon-emissions/

Staffell, I., Green, R., jan 2016. Is There Still Merit in the Merit Order Stack? The Impact of Dynamic Constraints on Optimal Plant Mix. IEEE Transactions on Power Systems 31 (1), 43–53.

Vaca, S. M., Patsios, C., Taylor, P., nov 2017. Enhancing frequency response of wind farms using hybrid energy storage systems. In: 2016 IEEE International Conference on Renewable Energy Research and Applications, ICRERA 2016. IEEE, pp. 325–329.

Vijayakumar, M., Li, L., Graff, G., Liu, J., Zhang, H., Yang, Z., Hu, J. Z., apr 2011. Towards understanding the poor thermal stability of V5+electrolyte solution in Vanadium Redox Flow Batteries. Journal of Power Sources 196 (7), 3669–3672.

Viswanathan, V., Crawford, A., Stephenson, D., Kim, S., Wang, W., Li, B., Coffey, G., Thomsen, E., Graff, G., Balducci, P., Kintner-Meyer, M., Sprenkle, V., 2014. Cost and performance model for redox flow batteries. Journal of Power Sources 247, 1040–1051.

Wei, L., Wu, M. C., Zhao, T. S., Zeng, Y. K., Ren, Y. X., apr 2018. An aqueous alkaline battery consisting of inexpensive all-iron redox chemistries for large-scale energy storage. Applied Energy 215, 98–105.

Wei, L., Zhao, T. S., Xu, Q., Zhou, X. L., Zhang, Z. H., mar 2017. In-situ investigation of hydrogen evolution behavior in vanadium redox flow batteries. Applied Energy 190, 1112–1118.

Yuan, Z., Duan, Y., Zhang, H., Li, X., Zhang, H., Vankelecom, I., feb 2016. Advanced porous membranes with ultra-high selectivity and stability for vanadium flow batteries. Energy and Environmental Science 9 (2), 441–447.

Zeng, Y., Li, F., Lu, F., Zhou, X., Yuan, Y., Cao, X., Xiang, B., mar 2019. A hierarchical interdigitated flow field design for scale-up of high-performance redox flow batteries. Applied Energy 238, 435–441.